CAUSAL CONDITION MONITORING FOR AXIAL PISTON PUMPS: PREDICTION OF DIFFERENT FAULTS UNDER VARIABLE OPERATING CONDITIONS

Svenja Horn, Ahmed Shorbagy, Michael Lenz, Simon Knoll, Moritz Winter, and Prof. Jürgen Weber

Institute of Mechatronic Engineering, Technische Universität Dresden,
E-mail: svenja.horn@tu-dresden.de, fluidtronik@mailbox.tu-dresden.de

Abstract.

The paper discusses a method for a targeted condition monitoring approach on key components of an axial piston pump. Three typical types of damage to an axial piston pump – valve plate cavitation, slipper wear and axial slipper-piston clearance - are artificially generated as realistically as possible. A variety of sensors were used to collect data on efficiencies, flow rates, temperatures, and accelerations of the new and the worn pump for 100 different operating conditions. The data was processed using signal analysis techniques to understand the influence of faults on the readings from different sensors. Two different machine learning algorithms – the support vector machine (SVM) and a gradient boost algorithm (XGBoost) - were used for fault detection. Several studies have been carried out to investigate which sensor gives the best accuracy and how many features are needed. This paper presents the first step towards a transferable and scalable condition monitoring concept, which should include the causal relationship between wear and load history to enable prediction of remaining life.

Keywords. Axial piston pumps, condition monitoring, machine learning, predictive maintenance, transferability, remaining lifetime.

1. INTRODUCTION

The ability to record large amounts of operating data with minimal effort and process it with intelligent algorithms opens up new ways for fluid technology, enhancing our understanding of component and system processes. This leads to a sustainable increase in the quality of future engineering and maintenance strategies. Current preventive maintenance guidelines prescribe the replacement of components at regular intervals to prevent spontaneous failures. While this approach improves failure safety, it causes high costs for the manufacture, replacement and disposal of components, as these parts often need to be replaced long before reaching their actual service life and are also designed to be oversized.
Predictive maintenance (PM) concepts aim to eliminate these disadvantages and enable needs-based, optimal maintenance. This requires knowledge of the current and past status of each component in the system, also known as condition monitoring (CM), and relating

this to process and machine data. Classic CM evaluates the wear tendencies to predict when technical usability is no longer guaranteed. Additionally, correlating wear with load history will allow, for the first time, causal statements about the reason for failure and the predictions of the remaining life.
This paper presents the first steps towards this vision, starting with the artificial wear of three pump parts in chapter 3. It explains in detail the artificial cavitation of the valve plate, the wear of the slipper sealing land, and the axial clearance between slipper and piston. Chapter 4 provides an overview of the measurement setup, the installed sensors and the measurement procedure. It concludes with measurement results showing the impact of the faults on the efficiencies, as well as a closer examination of the signal from the triax-y accelerometer in time and frequency domain. In Chapter 5, the data-driven analysis is explained, beginning with the pre-processing of the data, providing an overview of the feature engineering, and finally presenting the results of the model evaluation.

2. STATE OF THE ART

Table 1 provides an extensive overview of the literature on condition monitoring (CM) in axial piston pump systems, aiming to categorize and summarize key findings in a structured manner. The black bars are set to a maximum value to improve the visibility of the variation in the lower range, set to 16 for the column of operating conditions for example.

The literature review is organized into the following five main categories: investigated faults, data acquisition methods, employment of machine learning (ML) and CM techniques, and a judgment on predictive maintenance (PM) status. The first column in the table denotes the references to the literature sources, providing a comprehensive list of the studies reviewed. The second column categorizes the pump types, with the main focus on Axial Piston Units (APU). The subsequent block of the table details the investigated faults, divided into the components where the faults are applied, such as valve plate, slipper, or bearing faults. The number of fault levels investigated across all fault types is also given, offering insights into the scope and depth of fault analysis conducted in the literature. The section on data acquisition methods outlines the sensors used for measurements, along with the total number of sensors employed and the number of operating conditions considered. This provides a comprehensive understanding of the data collection strategies adopted in the reviewed studies. Regarding ML methods, “class” and “value” stand for using a classification or a regression algorithm. Additionally, it indicates whether ML or deep learning (DL) techniques were utilized to achieve these goals. An approach is classified as DL if it does not require separate feature extraction and engineering, as is often the case with various types of neural networks.

CM methods are classified into three categories: knowledge-based CM with ML/DL, functional CM integrating functional statistics of measurement data, and model-based CM incorporating digital twin concepts. This classification follows the VDI norm 2888 /Vdi99/, dividing diagnostic methods for data evaluation into functional, knowledge-based and model-based approaches, see **Figure 1**. The model-based approach is primarily used for system analyses, such as in investigations on valve-controlled drives, e.g. by /Chi04, Ise06, Kre02, Kho97, Mün06a+b, -07a+b, Raz07/ using parity equations or parameter estimates. For displacement units, the functional approach is particularly suitable, as it is based on the periodic signals of rotary machines. Such signal-based procedures are already used as

standard in the monitoring of rolling bearings, e.g., in wind turbines /Hac07, Wir04/. The knowledge-based approach mainly uses pattern recognition methods and processes input and output data with a learning algorithm without information about internal system correlations. Pure knowledge-based methods use vast amounts of field data to draw conclusions about the use and wear of a machine. The knowledge gained remains within the company and is not published. While the knowledge-based approach may provide general and imprecise estimates, robust and transferable algorithms can cope with the high variety of system and environmental influences, as demonstrated in the works of /Tor11/, /Cas19a,b/. This project aims to combine the advantages of functional methods with those of knowledge-based methods.

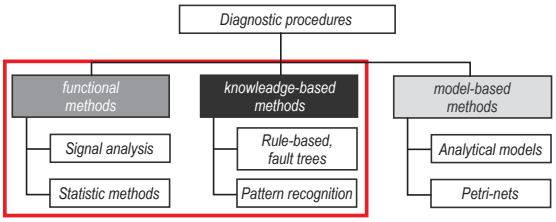

Figure 1: Classification of diagnostic procedures according to VDI standard 2888

Finally, Table 1 provides an assessment of PM status, offering an outlook on the transferability and remaining lifetime aspects of the CM approaches discussed in the literature.

Recent studies have aimed to optimize signal preprocessing by utilizing original sensor data in both time and frequency domains. They converted time series into Continuous Wavelet Transform (CWT) diagrams depicted in **Figure 2** and applied Deep Learning (DL) algorithms for analysis. Additionally, they've used Bayesian optimization to fine-tune Convolutional Neural Network (CNN) hyperparameters /Tan22, Tan24, Zhu23/.

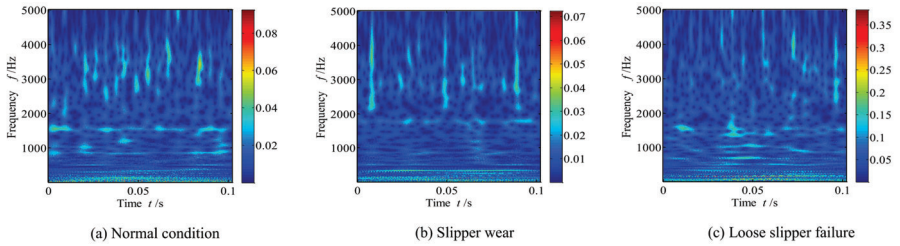

Figure 2: Continuous Wavelet Transformation (CWT) representation of vibration signal for CNN model /Tan22/

Another novel approach is the use of physics informed machine learning (PIML), which promises a better interpretation of the algorithm results. For this purpose, /Zhi23/ combines a neuronal network with the mass conservation equation in the exhaust pipe for different piston wear levels.

Table 1: Systematic literature overview of implementing CM in APUs

		Faults							Data Acquisition									ML methods		CM methods			PM	
		fault types							sensors															
source	device	valve plate	slipper	bearing	piston	cylinder	other	fault levels	vibration	acoustics	pressure	torque	efficiency	speed	flowrate	SP angle	number of sensors	number of operating conditions	goal	ML/DL methods	using ML/DL	functional CM	model based CM	transferability	remaining lifetime
/Ali16/	other							0									1	-	value	ML	●			-	-
/Ali18/	other						●	1						●	●		1	1	class	-		●		+	-
/Pau18/	APU							-									-	-	-	-				-	-
/Lu11/	APU	●	●					2	●	●						●	1	1	class	DL	●			+	-
/Gao05/	APU	●	●					2	●	●							1	1	class	-			●	-	-
/Has12/	APU	●				●		0	●				●				-	-	class	-			●	-	-
/Tor11/	APU		●	●		●		6		●	●		●			●	2	3	class	ML + DL	●	●		+	-
/Elt14/	other						●	0						●			1	0	class	-		●		+	-
/Li05/	APU				●			2				●					1	1	class	-		●		++	-
/Opp07/	APU			●				10			●					●	20	12	class	-		●		++	-
/Cas18/	APU		●	●		●		2		●	●		●			●	2	4	class	-		●		+	-
/Cas19a/	APU	●	●			●		5	●	●			●			●	2	9	class	ML	●			+	-
/Bed18/	APU	●	●			●		5	●	●			●				5	9	class	-		●		++	-
/Tan22/	APU		●				●	5		●				●		●	1	5	class	DL	●			+	-
/Kum19/	APU				●			4				●					3	3	value	-			●	-	-
/Zhu23/	APU		●				●	5		●				●		●	3	0	class	DL	●			+	-
/Cha21/	APU	●			●	●		4	●			●	●			●	9	1	class	ML	●			+	++
/Kel22/	APU	●						5	●								5	4	class	ML	●			+	-
/Don23/	APU		●			●		2		●			●				1	1	value	-			●	-	+
/He22/	APU	●	●		●		●	4	●	●		●		●		●	2	16	class	DL	●			++	+
/Tan24/	APU		●				●	5		●				●		●	3	1	class	DL	●			+	-
/Zhi23/	APU				●			4				●					1	1	class	DL	●		●	++	+
/Gne23/	APU	●	●					5	●	●						●	6	96	class	ML	●			++	-
this approach	**APU**	●	●		●			7	●	●	●	●	●	●	●	●	**24**	**120**	**value**	**ML + DL**	●			**+**	**++**

To summarise, previous investigations on displacement units have limitations, as they are restricted to one pump size and a few operating points, and no systematic investigation of the minimum sensor configuration has been carried out to date. The last row of Table 1 gives the perspective for this research: The overall aim of this project is to develop transferable and intelligent algorithms that function as reliably as possible for a holistic recording of the component condition, including load history, and the necessary minimum requirements for data generation.

This paper presents the first steps towards that perspective. It shows the development of two methods to artificially wear pump parts: one to cavitate a valve plate and another to enlarge the clearance between piston and slipper. Furthermore, it presents the analysis of the measurement data and the process steps of the implemented machine learning algorithms. Finally, it includes first results of the classification of three faults in the pump with respect to different sensor configurations and a representative set of operating conditions (OCs).

3. ARTIFICIAL WEAR OF PUMP COMPONENTS

Based on customer service data from past malfunction incidents from multiple axial piston pump manufacturers a compilation of common damage types to axial piston units has been

generated. These damages were sorted according to the following criteria: the location of damage, the damage mechanism and the intensity of the damage. From this study three different damage types were selected: damage in the slipper-piston joint, simulating a mechanical deformation damage, a cavitated valve plate surface and a mechanically damaged slipper surface. All three faults were artificially implemented into new pump parts, ensuring realistic form and location, and are presented in detail in the following chapter.

3.1. Axial slipper-piston clearance

For simulating a damaged slipper-piston joint, augmented joint clearance was induced by axial tensioning on a Schenck PE 40L hydraulic tensile testing machine up to a suitable amount of plastic deformation of the slipper brass material.

In order to estimate the necessary axial force, a finite element analysis (FEA) of the process was performed, employing bilinear isotropic hardening models to account for material plasticity of the slipper and piston, with values for yield strength and the tangent modulus derived from material supplier certificates. **Figure 3 a)** shows the resulting equivalent plastic strain resulting at a remaining clearance of 2 mm, which was set in the analysis to obtain an upper bound for the tensile force. It is visible that plastification occurs solely in the much softer slipper material. The picture also shows the specially designed fixture that mounts the piston and slipper to the tensile machine without damaging functional surfaces, allowing for the application of a controlled displacement u. The polymer disc was introduced in the actual experimental setup to provide a bump stop when measuring clearance. Figure 3 b) shows the experimental setup of the hydraulic tensile testing machine.

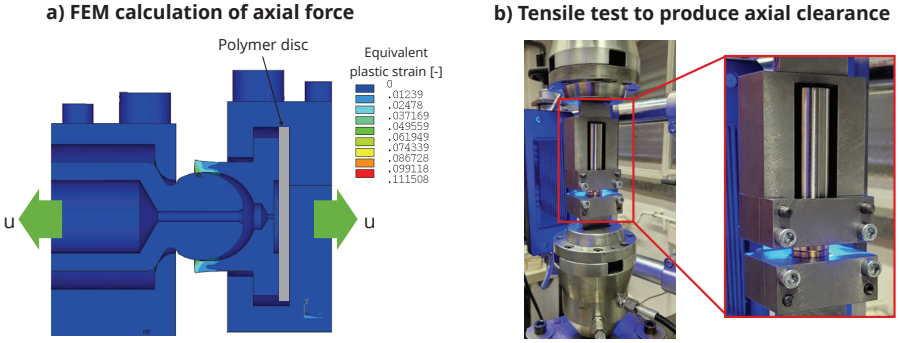

Figure 3: Simulation (left) and laboratory (right) setup for piston joint stretching

In a first run, an incremental step test of a slipper-piston assembly was performed, applying axial displacements of increasing magnitude to correlate the reaction force with the resulting permanent clearance, see **Figure 4 a)** and **b)**. In this context, measured clearance was defined as the axial deformation of the joint between -0.1 and 0.1 kN axial force.

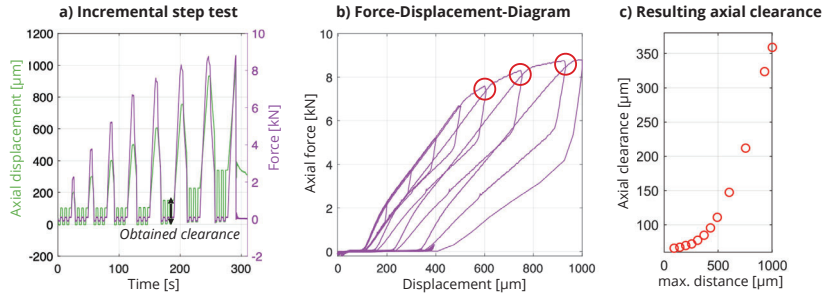

Figure 4: Incremental step cyclic loading of piston joint (left), force-displacement-diagram (middle) and obtained axial clearances (right)

A clearance of 180 µm was chosen to apply to the piston slipper assemblies, drawn from investigations of /Gne23/, in Figure 5 b). It was found that when subjecting new pistons to the force treatment, the resulting clearance did only roughly correspond to the function in Figure 4 b) and additional displacement had to be applied iteratively in order to achieve the desired clearance. At the same time, the reaction force after achieving the desired clearance was in the range of 10 to 11 kN, in contrast to the predicted 8 kN. Meanwhile, Figure 4 b) shows how during the cyclic run, the force appears to almost cap out below 9 kN for high deformation, approaching ideal plastic flow behaviour of the material. It is plausible that during cyclic loading and unloading the frictional contact attains a different configuration as compared to a straight loading ramp. Furthermore, material damage induced in the material during cyclic plastification is suspected. The marked regions in the diagram, where the axial force upon reloading does not reach the same value as during initial loading, point to either or a combination of these effects. A proper clarification will require further investigation and testing. The joint clearances obtained for ten pistons are depicted in **Figure 5 a).** A mean value of 179 µm was achieved, with a standard deviation of 7 µm. This compares to an initial mean clearance of 48 µm with a standard deviation of 11 µm. For the pump measurement, the outlier piston number 4 was discarded and the other nine were mounted, with an average clearance of 177 µm and a standard deviation of 3 µm. Figure 5 b) compares these values with those measured and reported in /Gne23/.

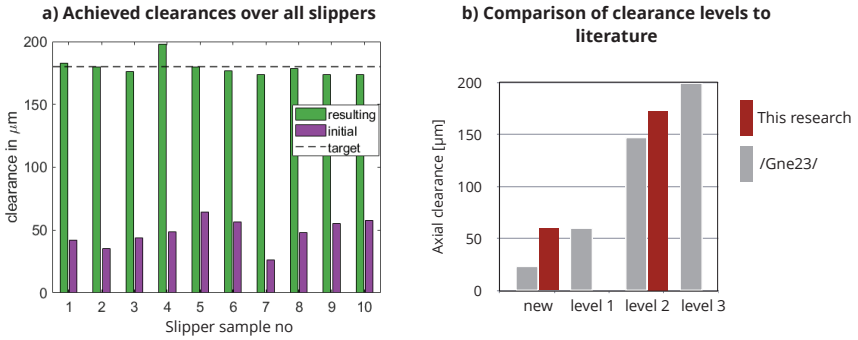

Figure 5: Obtained and initial values of axial clearance (left) and comparison to literature /Gne23/ (right)

3.2. Cavitated valve plate

Cavitation erosion damage on the surface of the valve plate is a very common damage especially in open-circuit pumps. In the case of a large damaged area on the valve plate, not only the volumetric efficiency is being affected, but also the pressure distribution over the entire surface of the valve plate, which leads to a change in the micro-motion of the cylinder block /Sho18/.

A computational fluid dynamics (CFD) model enables the localization of the cavitation erosion damage on the valve plate surface. The model predicts cavitation in the transition region between the high and low pressure kidneys of the valve plate. These locations were validated by deliberately inducing cavitation on the test rig after completion of the entire operating point grid. This was done by running the pump for at least 50 minutes at a speed of 2400 rpm, below its self-priming speed, and at a suction pressure of 0.9 bar absolute (the manufacturer's specification is 2300 rpm at 1.0 bar absolute to avoid cavitation). Good agreement was achieved between the predicted and the actual cavitation erosion damage locations.

After locating the cavitation erosion damage, different levels of damage were measured on several example valve plates from the field with a mean depth between 50 µm to 300 µm. Based on this study, three different damage levels are manufactured on three different valve plates. The manufacturing process is depicted in **Figure 6**. A mould with the location and shape of the fault was made. The mould was fixed to the surface of the valve plate to protect the surrounding areas. Using a high frequency sonotrode, the cavitation erosion damage was applied to the surface of the valve plate at three different intensities, see Figure 6 a). The surface measurement results qualify an excellent damage pattern corresponding to a real cavitation damage, compare Figure 6 b). In order to quantify the damage intensity of each valve plate, an optical surface measurement was performed. The surface measurement showed a clear correlation between the damage intensity and the volume removal of each valve plate, which is presented in Figure 6 c). Increasing damage intensity is associated with a rising volume removal.

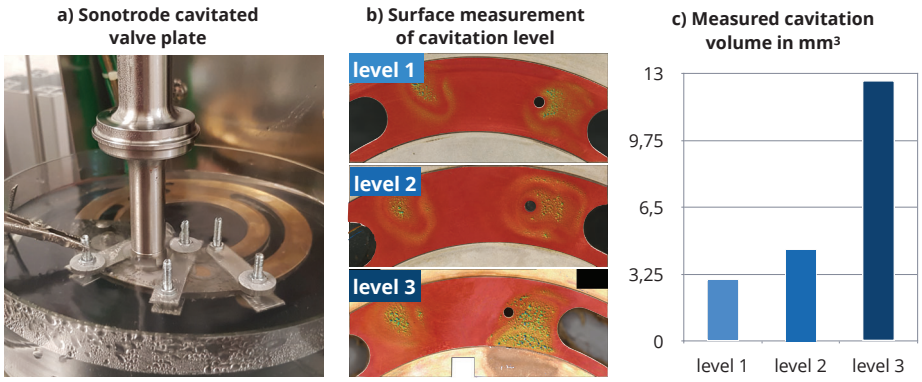

Figure 6: Artificial cavitation erosion damage on the valve plate surface

3.3. Worn slipper sealing land

A worn slipper sealing land produces an elevated leakage that decreases the volumetric efficiency. If the scratches of micro particles in the oil are deep enough, the entire hydrodynamic behaviour and the micro-motion of the slipper can be altered. This can lead to the destruction of the lubricating film between the slipper and the swash plate, resulting in increased friction and wear of the slipper /Iva20, 22/.

This fault was implemented manually using a filing tool. The target location, scratch shape and damage intensities were determined by analysing multiple worn slippers from different manufacturers. Filing was performed iteratively, with control of the achieved damage level by profilometer measurements. The result of an example surface scan is shown in **Figure 7**.

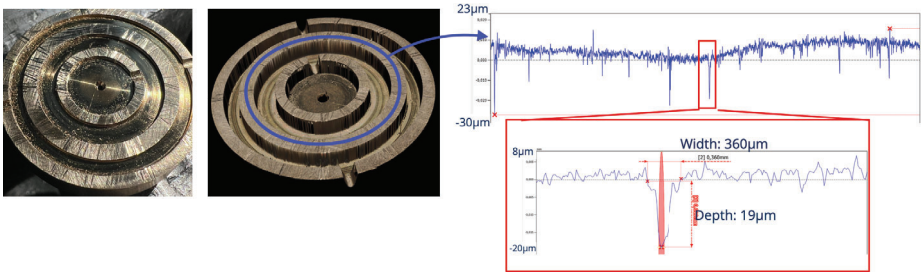

Figure 7: Artificial wear of slipper sealing land

4. EXPERIMENTAL

This section provides an overview and a detailed exploration of the test rig configuration, the sensors selected and positioned for data acquisition, followed by a description of the measurement procedure. The performance losses of the pump that can be attributed to the different faults are presented for several sensor data. For the triaxial accelerometer, the signal over one revolution in the time domain and the frequency spectrum are shown as example.

4.1. Test-Rig

A standard test rig setup capable of measuring pump characteristics was extended and modified. The upgraded version of the test rig used to perform the measurements was equipped with multiple sensors to capture high frequency pressure and acceleration signals. **Figure 8** shows a schematic of the hydraulic circuit of the test rig used.

This set-up of the test rig includes a suction pressure control to prime the specimen. A suction pressure of 1.8 bar was set to ensure that cavitation is avoided over the entire operating range. The implemented temperature control system helps to maintain a defined, consistent oil viscosity. The return flow is cooled by a heat exchanger and, if required, the oil in the tank can be heated by two electric heating cartridges. A coupling connects the pump to a variable speed electric motor with a maximum power rating of 270 kW. A torque transducer is also installed to measure the mechanical performance of the pump. Pressure and temperature sensors were strategically placed near the pump to facilitate accurate measurement and control of the desired operating conditions.

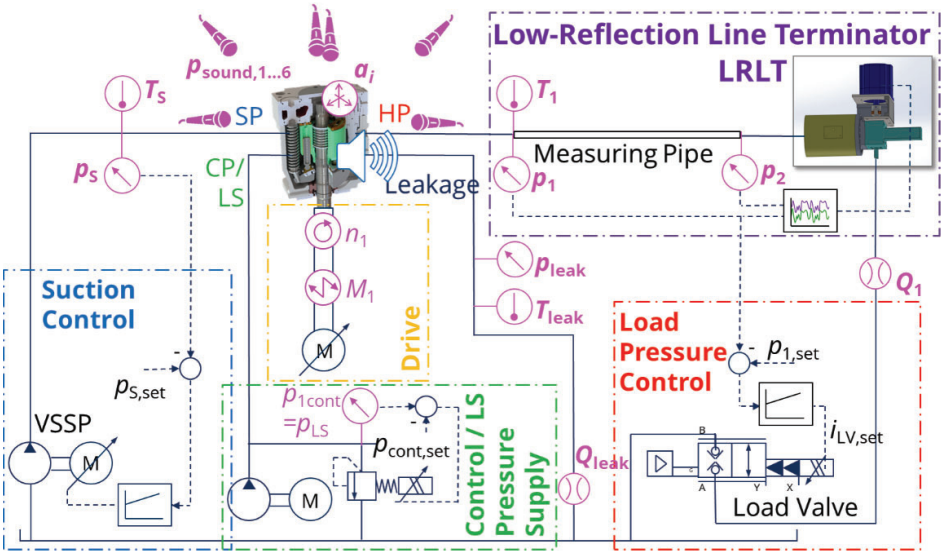

Figure 8: Hydraulic circuit of the pump test rig

A variety of high and low frequency sensors were used to monitor and record key parameters required for experimental analysis. **Figure 9** gives an overview of the installed sensors and their sampling frequency. The sensors were positioned to ensure accurate and reliable data acquisition. The pressure is recorded at high (HF) and low (LF) sampling rates. The sampling rate used for the evaluation for all high frequency sensors was 16.4 kHz.

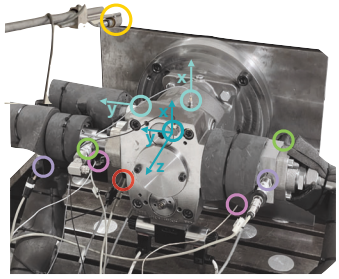

	Sensor	Sampling Frequency [kHz]	Location
	Acceleration Sensor	8	Pump casing, triaxial
	Acceleration Sensor	8	Pump casing, single Axis
	Pressure Sensor (HF)	25	Delivery & suction
	Pressure Sensor (LF)	1.2	Delivery, suction & leakage
	Temperature Sensor	0.3	Delivery, suction & eakage
	LVDT	16	Swash plate
	Microphones	50	According to DIN 45635

Figure 9: Overview on the installed sensors

4.2. Measurement Procedure

The pump measurements were carried out under different operating conditions using all available sensors. The measurements covered the entire operating range of the pump. In total, six pressure levels and four stroke angles were measured at four different speeds, resulting in 96 operating conditions. **Table 2** shows the reduced set of 28 OCs, that presents a representative selection to build and test the models. The findings of this paper are confined to the representative set, as a more sophisticated method, currently under development, is

being employed to reduce the features for the entire dataset due to the extensive number of features.

Table 2: Overview of representative set of 28 operating conditions (OCs)

100 %		75 %		50 %		25 %	
n [rpm]	Δp [bar]	n [rpm]	Δp [bar]	n [rpm]	Δp [bar]	n [rpm]	Δp [bar]
500	200	500	150	500	50	500	100
1000	100	500	250	1000	150	500	250
1000	250	1000	50	1000	300	500	300
1500	150	1000	200	1500	50	1000	150
1500	200	1500	100	1500	250	1500	50
2000	50	1500	300	2000	100	2000	200
2000	300	2000	150	2000	200	2000	250

In order to achieve a semi-equilibrium condition, a standby period of at least two minutes was allowed after setting up each operating point. The measurement period was chosen to be 10 seconds, which should be sufficient to capture several periodic motion cycles for each speed level. To maintain a constant oil viscosity and similar thermal conditions in the pump, the inlet temperature was regulated to 40°C+/-3°C for all measured operating conditions.

/Don23/ has shown that the flow pulsation changes due to faults, but is dependent on the pipeline length and therefore less transferable to other systems. In general, pressure pulsations emanating from a pump in a hydraulic system are influenced by reflections within the interconnected pipeline network. In the presented setup, a low reflection line terminator (LRLT) is used, which for each operating condition is steered to mimic the impedance of a pipeline of infinite length, thereby eliminating pressure pulsation reflections of the downstream hydraulic circuit. The LRLT guarantees that any change in pressure pulsations is attributed to the artificially added damage. This should ensure a robust transferability of the developed algorithm concerning the high pressure pulsation signal.

Initially, a reference measurement was conducted under healthy conditions without any damaged parts. This data serves as a baseline for comparison with subsequent measurements involving damaged parts. Each defect was measured separately, without combining multiple defects.

4.3. Performance Losses of the Pump due to worn components

This paragraph investigates the influence of wear on various performance parameters, including efficiencies, temperatures, and leakage, across the entire operating range. Mean values under different operating conditions are compared and depicted in Figure 10. The x-axis represents the operating conditions, sorted by increasing pressure blocks, each consisting of rising speed values.

Valve plate cavitation exhibits the lowest volumetric efficiency across all OCs. Since it does not have the lowest measured leakage, it can be assumed that internal leakage is also increased by valve plate cavitation, reducing the outlet volume flow. Simultaneously, valve plate cavitation shows the highest hydromechanical efficiencies. It is evident and physically expected that increased leakage occurs for all three types of wear. Slipper wear, in particular, negatively impacts friction losses, as indicated by lower hydromechanical efficiencies. This study provides insights into the relationship between wear-induced changes and hydraulic system performance, offering valuable information for predictive modelling and optimization strategies.

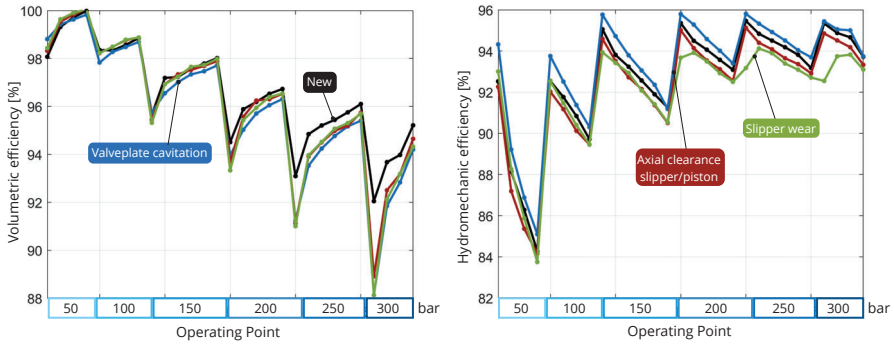

Figure 10: Influence of the faults on the volumetric and hydromechanic efficiencies over a broad operating range with rising speed for each pressure block

To understand the impact of the faults on different sensor signals, the data was evaluated in both the time and frequency domains. **Figure 11** exemplifies the accelerations of the triaxial-Y sensor over one revolution (left) and the corresponding FFT spectrum over 10 pump orders (right) for 500 rpm, 300 bar and 100 %.

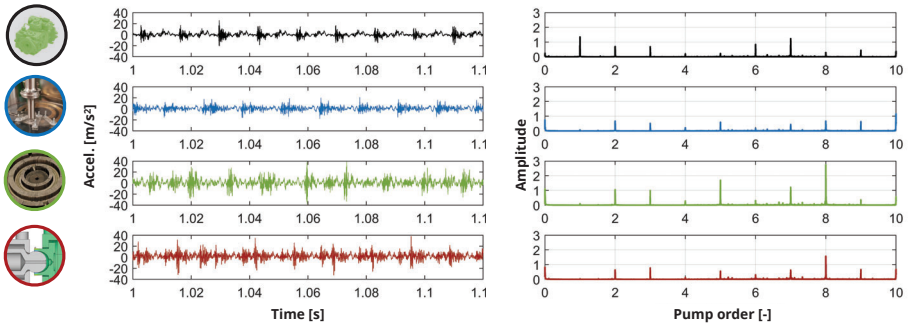

Figure 11: Accelerations over one revolution (left) and FFT (right) signal of the triaxial-Y sensor for 500 rpm, 300 bar and 100 %

While the new pump (first row in black) exhibits a dominant first pump harmonic resulting from the nine pulsating pistons, this harmonic is absent in the faulty signals. However, this observation is not consistent across all measurements; compare the results at 2000 rpm, 200 bar and 50 % in Appendix A, which display a completely different frequency spectrum.

In the time domain, higher amplitudes are observed for the slipper wear and the slipper-piston clearance fault, which is similar to the results in Appendix A. These examples illustrate the challenges of manual feature extraction and suggest the use of a powerful extraction tool like the TSFresh algorithm, which is used further in Chapter 5.

5. DATA-DRIVEN ANALYSIS

Figure 12 provides an overview of the individual steps for implementing ML algorithms. While all details about the data acquisition are described in chapter 4, the pre-processing of the data, the feature engineering and the model evaluation are explained in the next sections.

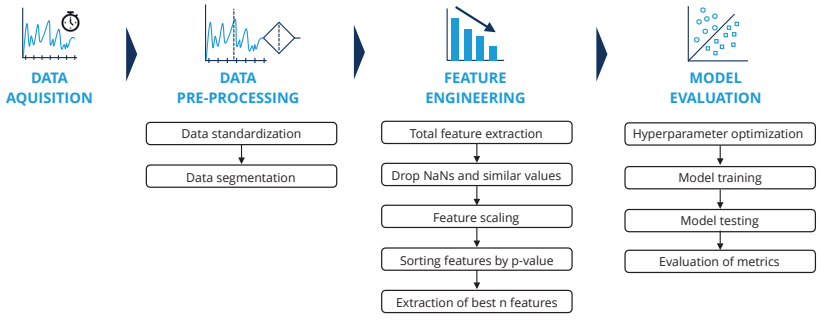

Figure 12: Methodical approach and individual steps for implementing ML algorithms

5.1. Pre-processing of the measurement data

The first step of data pre-processing involves formatting the measurement data into structures and file types that are accessible by the python-based algorithm. This includes segmenting the data and recombining it into new tables. In the rotary environment of an axial piston pump, effects of wear mostly appear cyclostationary, occurring with each revolution of the cylinder block or each piston (in this case nine times per revolution). Hence, the characteristic segment length depends on the speed of the pump. Longer time segments contain more precise information about repeating patterns or non-random anomalies. At the same time, to provide more information for training the algorithm, it is better to have as many segments as possible. The characteristic time segment length is chosen as twice the length of the inverted characteristic fault frequency, in which patterns and anomalies occur. It is calculated by equation 5.1, using the nominal speed of each OC $n_{OC,\mathrm{nominal}}$.

$$\Delta t_{\mathrm{seg}} = \frac{2 * 60 \frac{s}{min}}{n_{OC,\mathrm{nominal}}} \tag{5.1}$$

To ensure that all OCs are weighted equally, the number of time segments is set to 80. Unfortunately, the measurements at 500 rpm only contain 40 segments and are therefore slightly under-represented. Different sensors record different measurement ranges that may distort the calculation of the features. It is therefore common practice to standardise the raw data, carried out with the StandardScaler from the scikit-learn library centralizing the data around zero.

5.2. Feature extraction and evaluation

TSFresh is used to extract features from the time series /Chr18/. To ensure equal weighting of all features, a transformation into a common space is performed with the StandardScaler. Depending on the number of operating conditions and sensors, several hundred to thousands of features are calculated. For the vision of an onboard sensor system with microelectronics, minimizing the number of features is advantageous in terms of hardware requirements and computing time. Additionally, a balance needs to be found between fewer features for better generalization and more features for higher model accuracy.

The p-value is used to calculate the significance of each feature. Low p-values indicate a high importance of features for recognizing wear types by rejecting the null hypothesis. Furthermore, the significance of these features is evaluated using the Benjamini-Hochberg procedure /Ben95/. The procedure excludes irrelevant features from the analysis. The retained features in the relevance table are sorted by increasing p-value. **Figure 13** shows the best p-valued features for sets of [20, 50, 100, 200] features sorted by high and low frequency sensors for a set of 28 OCs, refer to Table 2. Over all feature sets, the high pressure sensor and the triaxial acceleration sensor contain the most important information, latter particularly in x and y directions. For higher numbers of features, sensors sampled at low frequencies also contain relevant information.

It should be noted that the p-value only provides a local correlation of *one* feature to the wear prediction and therefore allows only a rough estimate of its importance. The final accuracies of different feature sets can deviate from this, as they take into account the global relationships between many features and their interactions. Thus, features with lower p-values might not always result in the highest model accuracy when considered within the context of other features.

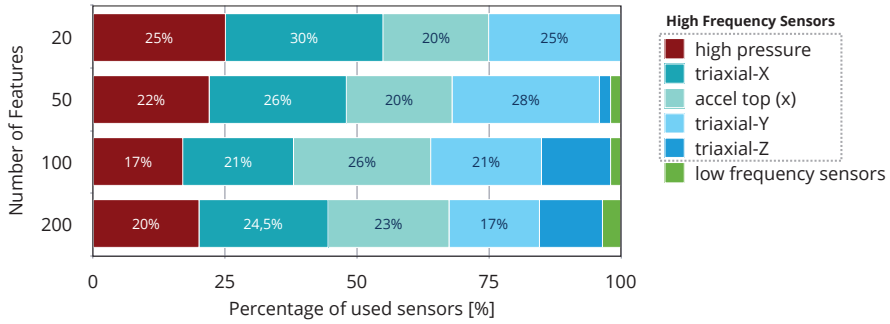

Figure 13: Best p-valued features for sets of [20, 50, 100, 200] features sorted by sensors

5.3. Model evaluation for fault detection

Many different algorithms for classifying features have been extensively developed, tested, and compared in the literature. Generally, a decision must be made whether to select a deep learning or a machine learning algorithm. Deep learning algorithms are excellent for large datasets, making them particularly advantageous for field data. They are complex to develop and can manage diverse types of data, unlike the simpler datasets examined in this study.

For this study, the two machine-learning algorithms, Support Vector Machine (SVM) and XGBoost, were chosen due to their power and robustness, while being relatively simple to implement and interpret. Both are supervised learning algorithms capable of wear type *classification* and wear depth *regression,* latter will be further investigated for valve plate cavitation levels.

SVM works by finding the hyperplane that best separates data points into different classes or predicts continuous outcomes. It aims to maximize the margin between classes, allowing for robust generalization to unseen data. By transforming input data into higher-dimensional feature spaces, SVM can effectively handle nonlinear relationships between variables. Additionally, SVM has regularization parameters that help prevent overfitting, making it suitable for datasets with high dimensionality and small sample sizes which is perfectly fitting to the data of this paper. SVM is popular in various machine learning applications and has been successfully applied to similar problems for the detection of faulty pumps parts (f.e. /Tor11, Cas19, Cha21/). XGBoost is a highly efficient and flexible implementation of gradient boosting. It builds an ensemble of decision trees sequentially, where each tree corrects the errors of the previous one, leading to highly accurate models. One of the key advantages of XGBoost is its robustness against overfitting, achieved through techniques such as regularization and shrinkage. Additionally, XGBoost is known for its scalability and speed, handling large-scale data efficiently.

For the hyperparameter optimization the optuna library is used. It is based on a bayesian optimization algorithm called “Tree-structured Parzen Estimator”. The hyperparameter optimization is performed on the total feature set of all sensors for the representative 28 OCs. The hyperparameters are used for all further accuracy calculations. A test of a further hyperparameter optimization for the 700 features of the high pressure sensor did not achieve any significant improvements in accuracy.

It is assumed that during one OC the features in the measurement data are very similar. If models are both trained and evaluated on the basis of this very similar data of the same set of OCs, overfitting to the given data cannot be ruled out. To prevent overfitting, the “GroupKFold” cross-validation strategy is therefore used. It ensures that the features from one OC occur either in the training or in the test data set, but not in both data sets at the same time. The data is split into training and test data with a typical amount of twenty percent proportion of test data using ten folds. To investigate the generalization of the results, the folds containing a different set of training and test data are calculated along with the corresponding accuracy results.

Figure 14 (left) provides a boxplot of the mean accuracies and their dispersion of different sensors, with a limitation of 700 features for both estimators, SVC and XGBC. Using all components of the triaxial acceleration sensor results in perfect fault prediction for the limited amount of test data. When examining the individual components (x, y and z), the data from the y-component of the triaxial sensor provides very high accuracy, also compared to the uniaxial acceleration sensors and the high-pressure sensor. The reason for those differences are not yet conclusively determined. One possible explanation, regarding the valve plate cavitation, is that cavitation influences the pressure build-up in the piston, thereby affecting the forces and torques on block and valve plate. Due to the torque

characteristics, this pump experiences significant torque fluctuations around the y-axis, which could be altered by the faults. Further investigations are pending.

The right plot in **Figure 14** shows the accuracy of the triaxial-Y sensor depending on the number of features. The SVC model already provides very high accuracies over 95 % for feature sets with more than 10 features, while the XGBC model achieves similarly high accuracy with more than 20 features.

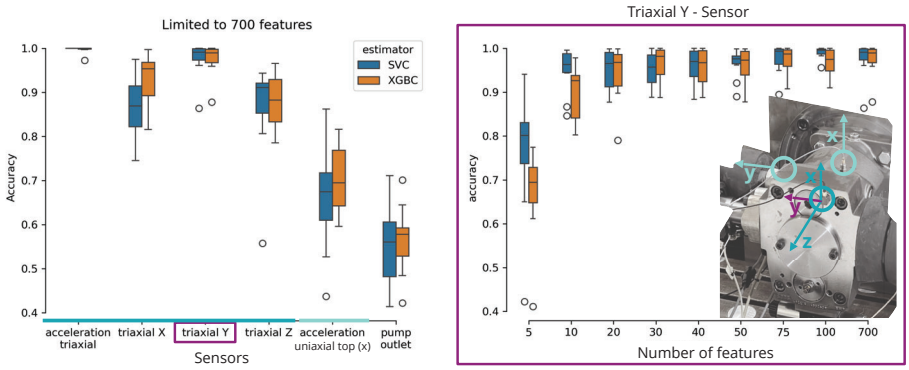

Figure 14: Accuracy results for different sensors with a total of 700 features (left) and accuracy results for different numbers of features of the triaxial-Y sensor (right)

The learning curves of both, the entire set of all features and sensors as well as the reduced set of 20 features of the triaxial-Y sensor are provided in appendix B showing that both models are not overfitted and well generalised.

6. SUMMARY AND OUTLOOK

This paper explains in detail how targeted and realistic artificial wear is applied to the valve plate, the slipper surface and the slipper-piston joint of an axial piston pump. With a sonotrode, cavitation has been applied to the valve plate surface in the area of the transition between low and high pressure. Axial clearance between slipper and piston of precisely defined values has been induced on a tensile test machine. A typical wear pattern was added to the slipper surface by filing.

Pump measurements have been conducted over a wide range of 96 operating conditions for each fault with a minimum of two repetitions. Results indicated that all faults resulted in higher leakage values and thus reduced volumetric efficiency. Notably, as valve plate cavitation progressed, volumetric efficiency decreased while hydromechanical efficiency increased, complicating system-side fault detection based on performance losses.

Feature extraction evaluation of a representative set of operating conditions (OCs) highlighted that the high-pressure sensor and accelerometers captured the most crucial information about the pump's condition. Further investigations will vary the set of OCs. The features are trained and tested with two algorithms, the SVC and the XGBoost, resulting in excellent accuracies of almost 100 % for the complete dataset of all sensors. Looking at the

results of single sensors, the triaxial-Y sensor achieves the best accuracies of 95 %, already for a small number of only 20 features.

The measurements were carried out under idealised conditions with constant inlet and outlet pressures and a constant inlet temperature. Such idealised conditions are not representative of the operating environments and could mean a deterioration in the prediction accuracies. Also, assembly and manufacturing tolerances may influence the results of the fault prediction. These controlled and reproducible conditions allow the investigation of defined disturbances on the model accuracies, which is planned for further development. Nevertheless, measurements on real machines in the field, collecting a large amount of data are necessary for a more general and robust model.

Regarding data segmentation across different OCs, low-speed conditions may be underrepresented due to their longer time periods per revolution, leading to fewer measurement segments compared to higher speed OCs. Future studies should select the same number of segments regardless of speed, increasing the measurement duration for low speeds to ensure a sufficient number of segments.

Further investigations include downsampling the sensor data within an optimization study to reduce sensor quantity and quality while determining the minimum sensor configuration and quality requirements necessary for maximum wear detection predictability. Measurements at different temperatures will provide more insights into data generalizability. The entire set of OCs will be analyzed, examining different subsets and their influence on prediction accuracy by various sensors.

The research aims to quantify multiple wear levels and types to achieve a comprehensive understanding of the degradation process in displacement units. Additionally, it will assess the transferability of developed monitoring techniques to other pumps of different sizes and manufacturers, ensuring broad industrial applicability. By addressing these objectives, this research aims to enhance the development of robust and adaptable condition monitoring strategies for displacement units, ultimately improving the reliability, efficiency, and lifespan of pump systems in industrial applications.

ACKNOWLEDGEMENT

The presented research activities are part of the project “Causal Condition Monitoring von Verdrängereinheiten durch Verschleiß- und Schadensdetektion in Korrelation zur Betriebs- und Lastsituation” (Ref. No. 22012 BR/1). The authors would like to thank the Fluid Power Research Fund of the VDMA for the funding and support.

Furthermore, a special thanks is given to Dr. Sven Werdin and the Institute of Solid Mechanics, TU Dresden, for facilitating machinery and guidance for the tensile test.

AUTHOR CONTRIBUTIONS

S.H. developed and organized the project concept. As the main author of the manuscript, S.H. was responsible for generating ideas and creating most of the figures and content. A.S. and M.L. conducted the investigation and implementation of the damaged pump parts. They were responsible for the setup and execution of the measurements and authored Chapter 3

and 4 of the manuscript. S.K. was responsible for feature analysis, hyperparameter optimization, model creation, training, and testing of the models. He also generated relevant figures. M.W. handled the data pre-processing using Matlab. J.W. was responsible for funding acquisition and supervision of the project. He provided critical revisions and valuable insights throughout the project.

APPENDIX A

Looking at the vibration levels of the three axes of the triaxial accelerometer over the entire operating range of the pump in **Figure 15**, it is clearly visible that the differences between the faults and the reference are more pronounced for the y and z direction. The trends suggest building two models, with one model exclusively classifying healthy from faulty and the second model identifying the fault. Different metrics could then also be used to evaluate the results and, for example, false-positive predictions could be penalized.

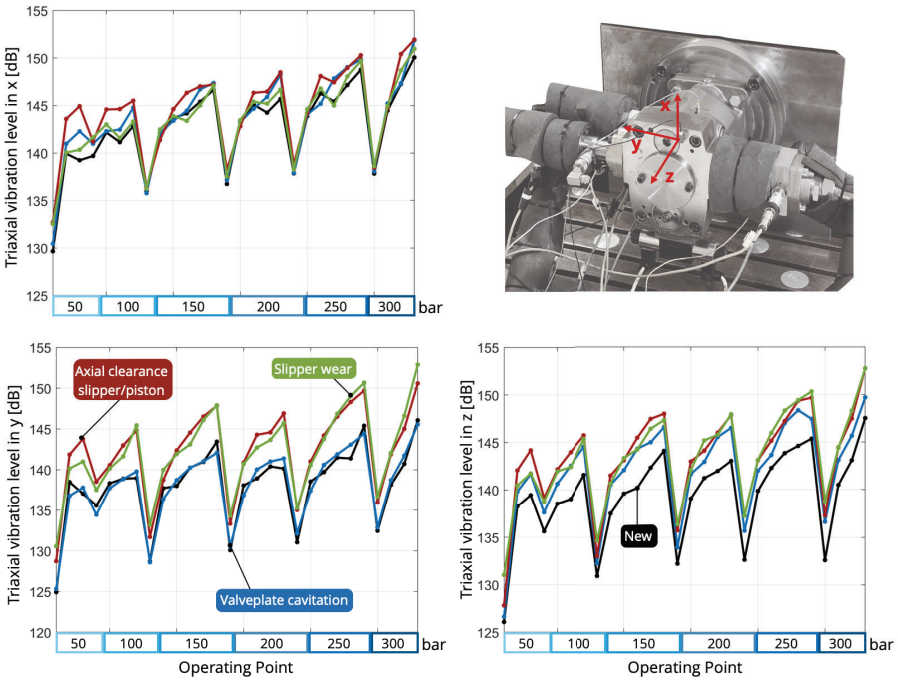

Figure 15: Influence of different faults on the three axes of the triaxial accelerometer

Figure 16 presents another example of signal analysis from the triaxial-Y accelerometer at 2000 rpm, 200 bar and 50 %. Notably, this sensor exhibits higher vibration levels for both slipper wear and axial clearance, consistent across all operating conditions shown in **Figure 15** and as previously observed in **Figure 11**. In the FFT spectrum, the pump order 8 stands out with a value of 27.7, more than three times higher than any other frequency.

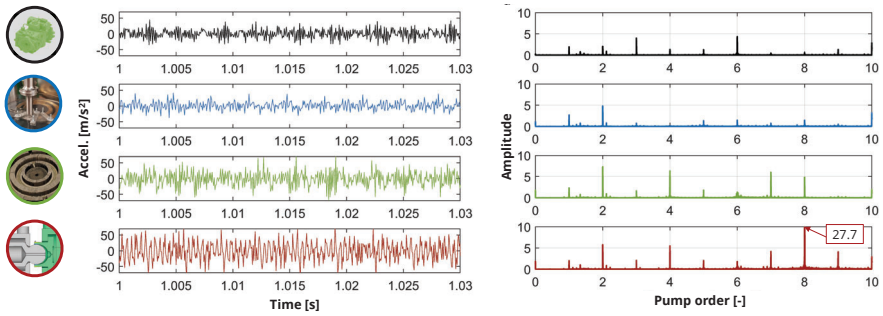

Figure 16: Accelerations over one revolution (left) and FFT (right) signal of the triaxial-Y sensor for 2000 rpm, 200 bar and 50 %

APPENDIX B

The learning curves of the support vector (SVC) and the XGBoost Classifier (XGBC) are depicted in **Figure 17** and **Figure 18**. In **Figure 17**, all of the several thousand features of all sensors are trained. Since the training and cross-validation accuracies are very close to each other and both values are very high, there is not much difference between the performance on the training data and the performance on the validation data. This indicates that the model is probably not overfitted but well generalised.

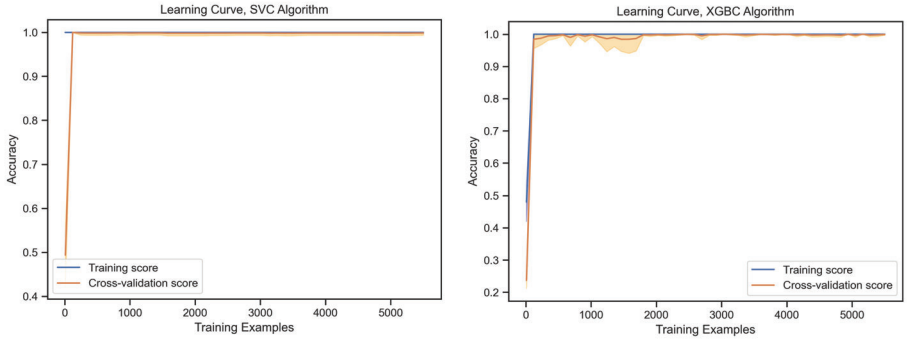

Figure 17: Learning curves of the SVC (left) and the XGBC (right) algorithm for the entire feature set of several thousand features of all sensors

Figure 18 shows the learning curve for the triaxial-Y acceleration sensor and a reduced feature set of the best p-valued 20 features each for one exemplary fold of the ten folds of the cross-validation. Reducing the number of features to 20 reduces the complexity of the model. This may result in the model being less able to fully learn the training data, but at the same time improve the ability to generalise to new data.

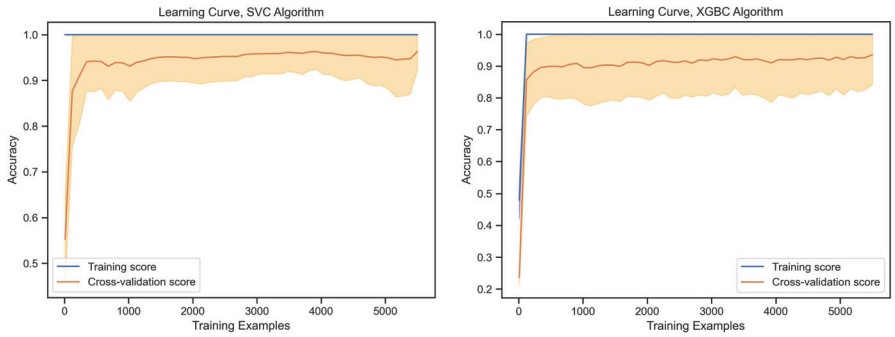

Figure 18: Learning curves of the SVC (left) and the XGBC (right) algorithm for the triaxial-Y acceleration sensor and a reduced feature set of the best p-valued 20 features

REFERENCES

/Ali16/ E. Ali, J. Weber, M. Wahler
A Machine Learning Approach for Tracking the Torque Losses in Internal Gear Pump - AC Motor Units, 10th International Fluid Power Conference, pp. 121–134, 2016.

/Ali18/ Emad Ali
Condition Monitoring of Wear Progress in Hydrostatic Pumps, International Journal of Trend in Scientific Research and Development, vol. 2, no. 6, pp. 139–142, 2018.

/Bed18/ A. Bedotti, M. Pastori, A. Lettini, P. Casoli
Condition Monitoring Based on Thermodynamic Efficiency Method for an Axial Piston Pump, Bath/ASME 2018 Symposium on Fluid Power & Motion Control, p. V001T01A004, 2018

/Ben95/ Y. Benjamini, Y. Hochberg
Controlling the False Discovery Rate: A Practical and Powerful Approach to Multiple Testing, Journal of the Royal Statistical Society: Series B (Methodological), Volume 57, Issue 1, Pages 289–300, Tel Aviv, 1995, https://doi.org/10.1111/j.2517-6161.1995.tb02031.x

/Cas18/ P. Casoli, A. Bedotti, F. Campanini, M. Pastori
A Methodology Based on Cyclostationary Analysis for Fault Detection of Hydraulic Axial Piston Pumps, *Energies*, vol. 11, no. 7, p. 1874, 2018

/Cas19a/ Casoli, P.; Pastori, M.; Scolari, F.; Rundo, M.
A Vibration Signal-Based Method for Fault Piston Pumps, In: *Energies*, 2019

/Cas19b/ Casoli P, Pastori M, Scolari F
A multi-fault diagnostic method based on acceleration signal for a hydraulic axial piston pump, AIP Conference Proceedings 2191, 020037 2019

/Cha21/ Q. Chao, Y. Shao, C. Liu, X. Yang
Health evaluation of axial piston pumps based on density weighted support vector data description, Reliability Engineering and System Safety, vol. 237, Sep. 2023

/Chi04/ Chinniah, Y.
Fault detection in the electrohydraulic actuator using extended Kalman Filter, Dissertation, University of Saskatchewan, 2004

/Chr18/ Christ, M., Braun, N., Neuffer, J., & Kempa-Liehr, A. W. (2018). Time Series FeatuRe Extraction on basis of Scalable Hypothesis tests (tsfresh – A Python package). *Neurocomputing*, *307*, 72–77. https://doi.org/10.1016/J.NEUCOM.2018.03.067

/Don23/ C. Dong, J. Tao, H. Sun, Q. Chao, C. Liu
Inverse transient analysis based calibration of surrogate pipeline model for fault simulation of axial piston pumps, Mechanical Systems and Signal Processing, vol. 205, Dec. 2023

/Elt14/ M. Eltabach
Condition monitoring of gear pumps using cyclostationarity, 9.IFK Aachen, 2014.

/Gao05/ Y. Gao, X. Kong, Q. Zhang
Wavelet Approach for Performance Monitoring and Diagnosis of a Hydraulic Pump, Proceedings of the 6th JFPS International Symposium on Fluid Power, Tsukuba, pp. 711–716, 2005.

/Gne23/ Gnepper, O., Hitzer, H., Enge-Rosenblatt, O.
Predictive Diagnosis in Axial Piston Pumps: A Study for High Frequency Condition Indicators Under Variable Operating Conditions, In: International Journal of Prognostics and Health Management, vol. 14, no. 1, 2023

/Hac07/ Hacke, B.; Reimers, E.; Hofmann, G.
Alles auf den Prüfstand – Neue Wege im Condition Monitoring, In: Antriebstechnik 12, 2007, S. 40 – 42

/Has12/ D. Hast, M. Gottfried, R. Findeisen,
A Method for the Interpretation of Parametric Faults in Model Based Condition Monitoring, vol. 45, no. 20. IFAC, 2012

/He22/ Y. He, H. Tang, Y. Ren, A. Kumar
A deep multi-signal fusion adversarial model based transfer learning and residual network for axial piston pump fault diagnosis, Elsevier B.V., Mar. 2022.

/Ise06/ Isermann, R.
Fault-diagnosis systems: an introduction from fault detection to fault tolerance, Berlin: Springer, 2006

/Iva20/ Ivantysyn, R.; Weber, J.; u.a.
Investigation of the Wear Behavior of the Slipper in an Axial Piston Pump by Means of Simulation and Measurement, 12. IFK 2020, Dresden, 2020

/Iva22/ Ivantysyn, R., Horn, S., Weber, J.
Design of a Lead-Free Slipper Bearing for Low Speed Axial Piston Pump Applications, In: IEEE GFPS 2022, 2022

/Kel22/ N. Keller, A. Sciancalepore, A. Vacca
Demonstrating a Condition Monitoring Process for Axial Piston Pumps with Damaged Valve Plates, International Journal of Fluid Power, vol. 23, no. 2, pp. 205–236, 2022

/Kho97/ Khoshzaban-Zavarehi, M.
Online condition monitoring and fault diagnosis in hydraulic system components using parameter estimation and pattern classification, Dissertation, University of British Columbia, Vancouver, 1997

/Kre02/ Kreß, R.
Robuste Fehlerdiagnoseverfahren zur Wartung und Serienabnahme elektrohydraulischer Aktuatoren, Dissertation, TU Darmstadt, 2002

/Kum19/ N. Kumar, R. Kumar, B. K. Sarkar, S. Maity
Condition monitoring of hydraulic transmission system with variable displacement axial piston pump and fixed displacement motor, in Materials Today: Proceedings, Elsevier Ltd, 2019, pp. 9758–9765.

/Li05/ Z. Li
Condition Monitoring of Axial Piston Pump, Master thesis at the University of Saskatchewan Saskatoon, no. November, p. 134, 2005, [Online]. Available: http://ecommons.usask.ca/bitstream/handle/10388/etd-11252005-202705/EricLithesis2005NovA.pdf

/Lu11/ C. Lu, N. Ma, Z. Wang
Fault detection for hydraulic pump based on chaotic parallel RBF network, EURASIP Journal on Advances in Signal Processing, pp. 1–10, 2011.

/Mün06a/ Münchhof, M.
Model-based fault management for a hydraulic servo axis, Dissertation, TU Darmstadt, 2006

/Mün06b/ Münchhof, M.
Model-based fault management for a hydraulic servo axis, In: The 5th International Fluid Power Conference (5. IFK), Bd. 3, S. 419-430, Aachen, 2006

/Mün07a/ Münchhof, M.
Fehlerdiagnose für hydraulische Servo-Achsen, In: Automatisierungstechnik, S. 96-103, 01/2007

/Mün07b/ Münchhof, M.
Modellbasierte Hydraulik-Überwachung - Übersicht über modellbasierte Verfahren zur Überwachung linearer Servo-Achsen, In: O+P Ölhydraulik & Pneumatik, S. 184-193, 04/2007

/Opp07/ M. Oppermann,
An investigation into failure prediction for mobile hydraulic systems, no. March. 2007.

/Pau18/ G. Paulmann, G. Mkadara
Condition monitoring on hydraulic pumps – lessons learnt, European Rotorcraft Forum (ERF 2017), p. 13, 2018.

/Raz07/ Razavi, B.
Condition monitoring in a hydraulic system of an industrial machine using unscented Kalman Filter, Master-Thesis, University of British Columbia, Vancouver, 2007

/Sho18/ Shorbagy A.; Ivantysyn R.; Weber J.
An experimental approach to simultaneously measure the temperature field and fluid film thickness in the cylinder block/valve plate gap of an axial piston pump. Proceedings of the 9th International Symposium On Turbulence, Heat and Mass Transfer, Rio de Janeiro, Brazil, 2018

/Tan22/ S. Tang, Y. Zhu, S. Yuan
Intelligent fault diagnosis of hydraulic piston pump based on deep learning and Bayesian optimization, ISA Transactions, vol. 129, pp. 555–563, Oct. 2022

/Tan24/ S. Tang, B. Cheong Khoo, Y. Zhu, K. Meng Lim, S. Yuan
A light deep adaptive framework toward fault diagnosis of a hydraulic piston pump, Applied Acoustics, vol. 217, Feb. 2024

/Tor11/ Torikka T.
Bewertung von Analyseverfahren zur Zustandsüberwachung einer Axialkolbenpumpe, Dissertation, Rheinisch-Westfälischen Technischen Hochschule Aachen, Fakultät für Maschinenwesen, Aachen, 2011

/Vdi99/ Verein deutscher Ingenieure
VDI 2888 1999-12, Zustandsorientierte Instandhaltung, Berlin, 1999

/Wir04/ Wirth, R.
Entwicklungstendenzen zur vollautomatischen Diagnose von Getriebeschäden, In: VDI Berichte 1826, 2004, S. 117 – 134

/Zhi23/ Z. Wang, Z. Zhou, W. Xu, C. Sun, R. Yan
Physics informed neural networks for fault severity identification of axial piston pumps, Journal of Manufacturing Systems, vol. 71, pp. 421–437, Dec. 2023

/Zhu23/ Y. Zhu, S. Tang, S. Yuan
Multiple-signal defect identification of hydraulic pump using an adaptive normalized model and S transform, Engineering Applications of Artificial Intelligence, vol. 124, Sep. 2023